Journal of Cleaner Production 164 (2017) 652–663

Contents lists available at ScienceDirect

Journal of Cleaner Production

journal homepage: www.elsevier.com/locate/jclepro

Facile synthesis of new amino-functionalized agrogenic hybrid composite clay adsorbents for phosphate capture and recovery from water

Emmanuel I. Unuabonah [a, *], Foluso O. Agunbiade [a], Moses O. Alfred [a], Thompson A. Adewumi [a], Chukwunonso P. Okoli [b, c], Martins O. Omorogie [a, b], Moses O. Akanbi [a], Augustine E. Ofomaja [b], Andreas Taubert [d]

[a] Environmental & Chemical Processes Research Laboratory, Department of Chemical Sciences, Redeemer's University, P.M.B 230, Ede, Osun State, Nigeria
[b] Adsorption & Catalysis Research Laboratory, Department of Chemistry, Vaal University of Technology, Private Bag X021, Andries Potgieter Boulevard, Vanderbijlpark, 1900, South Africa
[c] Analytical/Environmental Chemistry Unit, Department of Chemistry/Biochemistry, Federal University Ndufu-Alike Ikwo, Ebonyi State, Nigeria
[d] Institute of Chemistry, University of Potsdam, D-14476, Potsdam, Germany

ARTICLE INFO

Article history:
Received 28 January 2017
Received in revised form
23 May 2017
Accepted 17 June 2017
Available online 21 June 2017

Keywords:
Composite adsorbents
Sustainable
Phosphate recovery
Water
Desorption kinetics

ABSTRACT

New hybrid clay materials with good affinity for phosphate ions were developed from a combination of biomass-*Carica papaya* seeds (PS) and *Musa paradisiaca* (Plantain peels-PP), $ZnCl_2$ and Kaolinite clay to produce *i*PS-HYCA and *i*PP-HYCA composite adsorbents respectively. Functionalization of these adsorbents with an organosilane produced *N*PS-HYCA and *N*PP-HYCA composite adsorbents. The pH_{pzc} for the adsorbents were 7.83, 6.91, 7.66 and 6.55 for *i*PS-HYCA, *N*PS-HYCA, *i*PP-HYCA and *N*PP-HYCA respectively. Using the Brouer-Sotolongo isotherm model which best predict the adsorption capacity of composites for phosphate, *i*PP-HYCA, *i*PS-HYCA, *N*PP-HYCA, and *N*PS-HYCA composite adsorbents respectively. When compared with some commercial resins, the amino-functionalized adsorbents had better adsorption capacities. Furthermore, amino-functionalized adsorbents showed improved adsorption capacity and rate of phosphate uptake (as much as 40-fold), as well as retain 94% (for *N*PS-HYCA) and 84.1% (for *N*PP-HYCA) efficiency for phosphate adsorption after 5 adsorption-desorption cycles (96 h of adsorption time with 100 mg/L of phosphate ions) as against 37.5% (for *i*PS-HYCA) and 35% (for *i*PP-HYCA) under similar conditions. In 25 min desorption of phosphate ion attained equilibrium. These new amino-functionalized hybrid clay composite adsorbents, which were prepared by a simple means that is sustainable, have potentials for the efficient capture of phosphate ions from aqueous solution. They are quickly recovered from aqueous solution, non-biodegradable (unlike many biosorbent) with potentials to replace expensive adsorbents in the future. They have the further advantage of being useful in the recovery of phosphate for use in agriculture which could positively impact the global food security programme.

1. Introduction

The occurrence of some anions at desirable quantity is crucial to the environment, but the presence of these anions in the environment and the ingestion by humans at high concentrations could, however, be detrimental to both the environment and human health. For instance, anions such as phosphates and nitrates are essential nutrients for all life forms. They are crucial nutrients in the aqua system to maintain a reasonable level of productivity in lakes, rivers, and estuaries. However, high concentrations of phosphates and nitrates have been linked to eutrophication of water bodies and blue baby disease in infants (Oliveira et al., 2012; Bekele et al., 2014). There are point and non-point sources of phosphates in water which include discharge from industries and effluent from municipal sewage treatment plants and factories for the former and agricultural activities like runoff from farmlands treated with phosphate fertilizers, atmospheric deposition, and stormwater runoff for the later.

* Corresponding author.
E-mail addresses: unuabonahe@run.edu.ng, iyaemma@yahoo.com (E.I. Unuabonah).

http://dx.doi.org/10.1016/j.jclepro.2017.06.160
0959-6526/

Excess concentration of phosphates in surface water can lead to excessive algal growth followed by decomposition, depletion in dissolved oxygen, eutrophication and a reduction in water quality. Consumption of high concentrations of phosphate has been implicated in kidney damage and osteoporosis (Oliveira et al., 2012). It has been shown that continuous discharge of phosphate into a water body increases the level of toxins in such water body (Zhang et al., 2011).

In this regard, different approaches and technologies have been employed for removal of phosphates in water. These include biological treatment, chemical precipitation, and adsorption (Lin and Juang, 2002; Shen and Wang, 1994; Unuabonah et al., 2013). Biological treatment and chemical precipitation technologies are, however, not very efficient because of associated problems, such as; limited versatility, operational difficulties, the high cost of operation among others. Adsorption technique has been found to be more economical and efficient (Ugurlu and Salman, 1998) as it can also serve the purpose of nutrient recovery (Oladoja et al., 2015) especially in the face of depleting world supply of phosphate resources.

It is, therefore, important to look for cheap, versatile and efficient treatment technology which is applicable even in rural settings to remove anions from contaminated water. In this regard, the potentials of different adsorbents for the capture of phosphates in water have been investigated. Such adsorbents include fly ash, red mud, snail shell, hydrocalumite, (Huang et al., 2008; Oladoja et al., 2014; Ugurlu and Salman, 1998; Xie et al., 2015). However, these adsorbents were of low efficiency, adsorption capacity and rate of uptake of phosphate because of the non-functionalization of their surfaces.

In order to improve the efficiency and rate of phosphate uptake of these adsorbents used in environmental pollution control, several investigations have been dedicated to the surface functionalization of different mesoporous materials using aminoalkoxy silanes (Calvo et al., 2009; Hamoudi et al., 2010; Huang et al., 2008; Najafi et al., 2012; Puglisi et al., 2009; Xie et al., 2015). Furthermore, the uptake of several heavy metals such as mercury, lead, cobalt, copper and zinc cations (Lee et al., 2016; Najafi et al., 2012; Nakanishi et al., 2014; Xin et al., 2012), and even organic molecules (Ghorbani et al., 2016; Tu et al., 2015; Zhang et al., 2015) with amino-functionalized mesoporous materials have been well documented. The uptake of anions such as chromate, arsenate and selenate, nitrate and phosphate with protonated amino-functionalized mesoporous silicas has also been studied (Chen et al., 2015; Ebrahimi-Gatkash et al., 2015; Elwakeel et al., 2016; Morales et al., 2016). Even though there have been reports on the use of phosphate-modified clay adsorbents for removal of heavy metal ions (Adebowale et al., 2008; Olu-Owolabi and Unuabonah, 2011; Unuabonah et al., 2010), there is however, no report on the removal and recovery of phosphate from aqueous solution using amino-functionalized agrogenic based hybrid clay composite adsorbents.

In this present study, new amino-functionalized Zn-doped agrogenic-clay (Zn-HYCA) composite adsorbents were prepared from Kaolinite, *Carica papaya* seed and Plantain Peels (*Musa paradisiacal*), characterised and applied for phosphate ion removal in water. Microwave-assisted technique was used prior to amino-functionalization. It has been suggested that microwave irradiation provide efficient pre-treatment of biomass for adsorption (Simha et al., 2017). Amino-functionalization, aside from improving the adsorption capacity of the adsorbents for the adsorption of phosphate ions, enhanced the rate of uptake of phosphate and helped retain more of the adsorbents' capacity even after 5 adsorption-desorption cycles. The technique employed in the preparation of these adsorbents is simple and could be upscaled for large-scale treatment of water.

2. Materials and methods

2.1. Materials

Raw kaolinite clay was obtained from Redemption City, Ogun State, Nigeria and the *Carica papaya* seeds and plantain peels were collected from different locations in Nigeria. Zinc chloride, [3-(2-aminoethylamino) propyl] trimethoxysilane (AEPTS, $C_8H_{22}N_2O_2Si$, $\geq$ 80.0 wt%) were Sigma-Aldrich Chemie products; Toluene, Isopropanol, Potassium dihydrogen phosphate, Ammonium metavanadate, Ammonium molybdate hexahydrate, the Hydrochloric acid used were of analytical grade.

2.2. Methods

2.2.1. Preparation of hybrid clay adsorbents with microwave assisted method

Raw kaolinite clay was processed for the removal of stones and other heavy particles present in the sample. The clay material was purified according to the method described by Adebowale et al. (2005) via several washes and filtration processes with a 100 mesh size sieve after treatment with 30% H_2O_2. The biomasses (*Carica papaya,* and Plantain peels) were pretreated by sun drying until constant weight was obtained and subsequently pulverised. They were collected and stored in separate airtight containers.

Kaolinite, crushed *Carica papaya* seeds or plantain peels, and $ZnCl_2$ were weighed in the ratio (1:1:2) and thoroughly mixed in a beaker with 50 mL deionized water. The mixture was allowed to stand for 24 h with intermittent stirring and was subsequently dried in an oven. The impregnated mixture was transferred into a microwave transparent reactor, purged with nitrogen gas for about 5 min and calcined for 15 min at 450 W in a microwave oven (Kenwood model K30GSS13). The product was allowed to cool in a desiccator, washed with dilute HCl and washed several times with deionized water until a clear solution was observed. These materials were dried in an oven at 105 °C, cooled in the desiccator, packed in sample bottles and labelled as *i*PS-HYCA and *i*PP-HYCA composite adsorbents (where *PS* and *PP* represent *Carica papaya* seeds and Plantain Peels respectively).

2.2.2. Functionalization of adsorbents

The hybrid clay composite adsorbents *i*PS-HYCA and *i*PP-HYCA prepared were functionalized using the method described by Li et al. (2008). The materials were dried at 105 °C in an oven to remove adsorbed water molecules on the surface of the materials, and 10 g of the materials was stirred vigorously in toluene containing [3-(2-aminoethylamino) propyl] trimethoxysilane (AEPTS, $C_8H_{22}N_2O_2Si$, $\geq$ 80.0 wt%). The reactant mixture was refluxed at 100 °C for 6 h. The product was filtered and washed with 50 mL isopropanol, then dried at 50 °C. The amino groups on the surface of the materials were then activated via interaction with 0.1 M HCl for 6 h. This step is aimed at converting surface amino groups to ammonium moieties. The materials were washed to a neutral pH and dried to constant weight at 50 °C. The materials were packed and labelled as *N*PS-HYCA and *N*PP-HYCA composite adsorbents.

2.3. Physicochemical characterization

The crystallinity and mineralogical assemblage of the adsorbents were determined via X-ray diffraction (XRD). The X-ray diffraction patterns were recorded on a Siemens D-5000 X-ray Diffraction equipment from 3.0 to 70° 2θ at 0.02° s^{-1}. The surface morphology and elemental composition were determined by

scanning electron microscopy (SEM) equipped with energy dispersive X-ray (EDX). Scanning electron microscopy (SEM) was done on a JEOL JSM 6510 SEM fitted with an EDX spectrometer of Oxford (INCAx-act SN detector). Fourier transformed infrared spectroscopy (FTIR) spectra for the adsorbents prepared as well as the raw materials used for the preparation was obtained from Shimadzu FT-IR 8400S (class 1, Laser product) Spectrophotometer. The pH point of Zero charge (pH_{pzc}) was determined by using the salt addition method (Li et al., 2008) in which 0.03 g of the adsorbent materials interacted with 10 mL of 0.01 M sodium chloride solution with pH ranging of 2.0–12.0 for 24 h. After 24 h the final pH of the solution was recorded and subtracted from the initial pH values. The change in pH was plotted against the initial pH, and the pH at which the change in pH is equaled to zero was noted as the pH point of zero charge.

2.4. Batch adsorption studies

2.4.1. Kinetic studies

The batch adsorption kinetic studies were carried out by agitating 250 mL of 100 mg/L phosphate in a beaker containing 2 g of the adsorbent for 2 h at an initial pH of between 6.0 and 6.3 at room temperature of 30 °C. A 0.5 mL solution was withdrawn using a micropipette at a predetermined time interval (between 1 and 120 min). The samples were diluted to 5 mL mark and filtered. The residual phosphate concentration was determined using APHA 4500 P Vanadomolybdophosphoric acid method (Greenberg et al., 1992) via the addition of 1 mL of the colour developing reagent to 3.5 mL of the filtered sample, followed by the addition of 1 mL of deionized water. The absorbance was determined with Shimadzu UV-VIS spectrophotometer at a wavelength of 420 nm. The adsorption capacity, q_t (mg/g) was estimated using the mass balance relationship:

$$q_t = \frac{\left(C_i - C_f\right) \times V}{w} \tag{1}$$

where C_i and C_f are the initial and equilibrium concentrations (mg/L) of phosphate ions respectively, V is the volume of the solution (L), and w is the mass in grams (g) of dry adsorbent used.

2.4.2. Kinetic models

To understand the kinetics of the adsorption processes, the experimental data of the adsorption processes are usually fitted into rate equations or kinetic models. For the sake of this study, the experimental data obtained from kinetic studies were analysed with three kinetic models namely; the Pseudo first-order (PFOM), Pseudo second-order (PSOM) and the Bruoers-Sotolongo Fractal (BSF [n,α]) kinetic models. Details of these kinetic models are shown in Supporting Information document (S1.1-S1.3).

2.5. Equilibrium isotherm studies

For the isotherm studies, 0.02 g of the adsorbents was added to 50 mL of adsorbate solution (pH 6.0 at 30 °C) with a predetermined concentration range (between 5 and 200 mg/L). The reaction was continuously agitated on a Forma Scientific orbital shaker 416 (19600-35) for 2 h. After 2 h of interaction, the mixture was filtered, the residual concentration and adsorption capacity were determined as described in sections 2.4.1 and S.2.1–S2.4 respectively.

2.5.1. Adsorption isotherm models

To optimise the design of an adsorption system for the removal of adsorbates, it is important to establish the most appropriate correlation for the adsorption equilibrium curves. Various isotherm including Langmuir-Freundlich (LF), Freundlich, and Bruoers-Sotolongo (BS) isotherm equations have been used to describe the equilibrium nature and mechanism of adsorption. Details of these equations are shown in the Supporting information document (S2.1-S2.4).

All equilibrium and kinetic plots were made using KyPlot® version 2.0 software with the non-linear mathematical versions of the equilibrium and kinetic models. The software used the Quasi-Newton (least square) optimization tool for fitting the data to the models. The Normalized Deviation (ND) and Normalized Standard Deviation (NSD) were used to determine the model that best describe both kinetic and equilibrium data for the various adsorbents. The mathematical equations for ND and NSD (Ganesapillai and Simha, 2015) are:

$$\text{Normalized Deviation} = \frac{100}{N}\sum\left|\frac{q_{e(\exp)} - q_{e(pred)}}{q_{e(\exp)}}\right| \tag{2}$$

$$\text{Normalized Standard Deviation} = 100\sqrt{\frac{\sum\left(\left(q_{e(\exp)} - q_{e(pred)}\right)/q_{e(\exp)}\right)^2}{N}} \tag{3}$$

For equilibrium data, the separation factor was calculated using the mathematical equation:

$$R_L = \frac{1}{1 + bC_o} \tag{4}$$

where R_L is the dimensionless separator factor, b is the Langmuir constant and C_o is the initial concentration of phosphate ions in solution (mg/L.

2.6. Adsorption-desorption cycles

The adsorption-desorption cycle was studied using phosphate-loaded composites which were agitated with either 0.01 M or 0.1 M NaOH solution for 2 h in Erlenmeyer flasks to desorp the phosphate ions from the composites. After filtration and washing with deionized water, the composite adsorbents were dried at room temperature and acidified with 0.01 M HCl solution to reactivate the composite adsorbents. Adsorption was performed batch-wise in Erlenmeyer flasks placed on a temperature-regulated shaker under the following conditions; temperature, 30 °C; adsorbent loading, 0.1 g/L; initial phosphate concentration, 20 mg/L; and pH ca. 5.5. Agitation of samples was for 2 h before the mixtures were filtered with 0.45 μm filter papers for all the adsorption tests.

These steps represent the first adsorption-desorption cycle, which was followed by four other cycles using the same adsorption batch. Desorption capacity and Regeneration efficiency were calculated using the equation given below:

$$q_{t(desorbed)} = \frac{C_p V}{w} \tag{5}$$

where q_t is the desorption capacity (mg/g); C_p is the final concentration of adsorbate in desorption solution (mg/L), V = volume of desorption solution (L), and w is the weight of the adsorbent used for desorption (g.

The residual phosphate in desorbed solution was analyzed using APHAs Vanadomolybdophosphoric acid method. The absorbance was determined with Shimadzu UV-VIS spectrophotometer at the wavelength of 420 nm, and phosphate concentration was

calculated from the calibration plot.

2.6.1. First order two-site desorption kinetic model

$$C_M = C_1 \exp(-k_1 t) + C_2 \exp(-k_2 t) \quad (6)$$

where C_m is the concentration (mg/L) of phosphate ions adsorbed onto the composite adsorbents at time t, C_1 and C_2 are the concentrations ($t = 0$) of desorbed phosphate ions bound to sites 1 and 2 (mg/L) with first-order kinetic desorption rate constants, k_1 and k_2, (min^{-1}) respectively.

2.6.2. Modified Statistical Rate Theory (MSRT) Desorption Kinetic Model

$$q_t = q_{des} \exp(\alpha - k_{des} t) \quad (7)$$

where q_t is the amount desorbed at time t, q_{des} is the predicted amount of phosphate ions to be desorbed (mg/g), α is the SRT constant and k_{des} is the rate of desorption.

Fitting equations (6) and (7) to experimental desorption data was achieved by optimising values for C_1, C_2, k_1, k_2, k, q_{des}, and α using the KyPlot® version 2.0 software with the non-linear mathematical versions of the equilibrium and kinetic models. The software used the Quasi-Newton (least square) optimization tool for fitting the data to the models.

3. Results and discussion

3.1. Physicochemical analysis

3.1.1. Fourier transform infrared (FTIR)

Figure 1 shows the Fourier Transformed Infrared Spectra of various modified Kaolinite adsorbents (solvothermal synthetic materials - *i*PP-HYCA *and* *i*PS-HYCA and surface functionalized materials -*N*PP-HYCA *and* *N*PS-HYCA) used in this study. The Fourier Transform Infra-red spectra of the raw Kaolinite exhibited bands for —O-H stretching vibrations between 3698 and 3611 cm^{-1}. The —O-H groups in the octahedral surface, which forms interlayer weak hydrogen bonds with the oxygen present in the Si-O-Si of each layer were indicated by the peaks at 3698, 3659 and 3621 cm^{-1} (Vilar et al., 2007). Antisymmetric and symmetric coupling vibrations of —O-H were associated with the bands at 3698 and 3659 cm^{-1} respectively (Frost and Vassallo, 1996; Unuabonah et al. (2007a) while the inner surface —O-H symmetry was indicated by the peak at 3621 cm^{-1} (Farmer and Russell, 1964; Vilar et al., 2007). The —O-H stretching and bending vibrations of silanol + aluminol and absorbed water were indicated by the peaks at 3414 and 1620 cm^{-1} respectively. Bands at 1068 and 910 cm^{-1} correspond to the Si–O and Al–OH in-plane bending vibrations respectively (Moore and Reynolds, 1989; Ogundiran and Winjobi, 2015).

The Fourier Transformed Infrared (FTIR) spectra for the modified adsorbents showed characteristic peaks for -N-H stretching at 1620 cm^{-1} and Si-O- bending vibration at 1069 cm^{-1} similar to those identified in hybrid clay composite adsorbent (HYCA) previously prepared by Unuabonah et al. (2013). Considering the FT-IR spectra of the adsorbents modified under inert condition (N_2 atmosphere), *i*PS-HYCA and *i*PP-HYCA adsorbents, they show similar peaks to those found in raw kaolinite clay apart from the loss of the in-phase and out-phase surface hydroxyls (3698 cm^{-1}, 3659 cm^{-1}) and inner-hydroxyl (3621 cm^{-1}) peaks found in the spectrum of the raw kaolinite clay (Fig. 1). This may be due to the microwave high-temperature heating of kaolinite during its modification with biomasses. There is also a noticeable increase in the intensities of the band associated with the —O-H bending vibration at 1620 cm^{-1} which could be —O-H contribution from agrogenic biomasses (*Carica papaya* seeds and plantain peels) used in the modification of kaolinite.

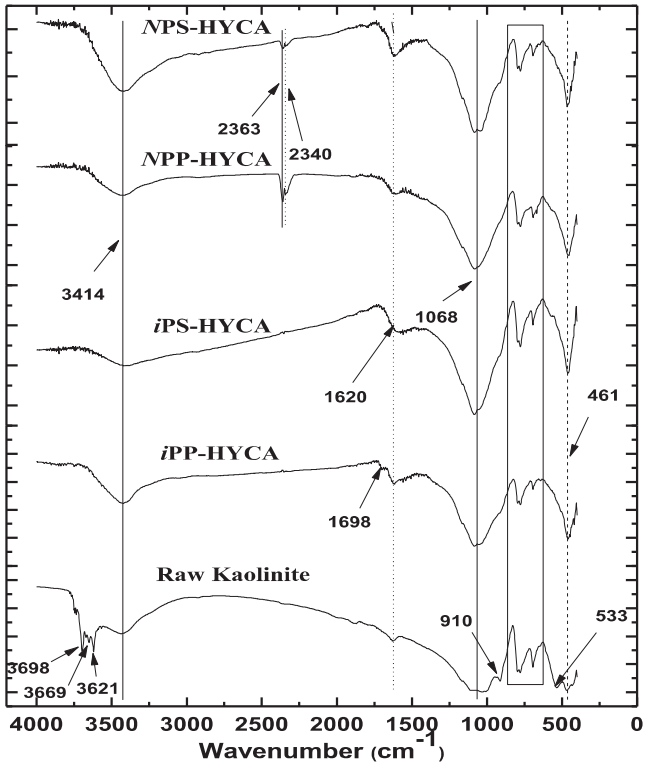

Fig. 1. FT-IR spectra of raw Kaolinite, microwave assisted solvothermal synthetic materials (*i*PP-HYCA *and* *i*PS-HYCA) and surface functionalized materials (*N*PP-HYCA, *N*PS-HYCA).

Furthermore, the spectrum of *i*PP-HYCA adsorbent presents a new peak at 1698 cm^{-1} indicating the presence of -C=O in the adsorbent(Bello et al., 2012). The spectra of all the modified adsorbents exhibit a strong band at 3414 cm^{-1} which suggest the presence of a combination of -N-H/-O-H stretching vibrations (Vilar et al., 2007) which may have formed —N-H·····O-Si (Cheng et al., 2012). The presence of NH_3^+·····O-Si is observed at 1620 cm^{-1} (Bacsik et al., 2011). The presence of —N-H in these adsorbents is further supported by the peak at 679 cm^{-1} for —N-H bending vibration (Adebowale et al., 2005). The —O-H is possibly a combination of that from the silanol (Vilar et al., 2007) in the clay and those from phenolics and carboxylic acid in the agrogenic biomasses (Vilar et al., 2007). The peak around 773 cm^{-1} suggests Si-O-Si vibrations associated with the formation of condensed silica structure (Adebowale et al., 2005). The band at 447 cm^{-1} confirms the presence of ZnO (Raevskaya et al., 2014) in the modified samples resulting from the use of $ZnCl_2$ in preparing the adsorbents.

For the amino functionalized adsorbents, *NPS-HYCA* and *N*PP-HYCA, similar spectra were observed when compared with those of raw kaolinite and adsorbents prepared under inert condition (*i*PS-HYCA and *i*PP-HYCA) as shown in Fig. 1, except for the development of new peaks at 2340 and 2363 cm^{-1} (Fig. 1) that are indicative of the presence of $-C=NH^+$ stretching vibrations (Attia et al., 2015).

3.2. Scanning electron microscopy (SEM) analysis

3.2.1. SEM image analysis

Fig. 2 shows the SEM images of *i*PS-HYCA, *N*PS-HYCA, *i*PP-HYCA and *N*PP-HYCA adsorbents. The SEM images for the adsorbents demonstrated that the shapes and sizes of their particles were irregular and heterogeneously distributed. The average particle size of the adsorbents (ca. 0.5 μm measured from the SEM EDX equipment) was above those of nanomaterials. Hence, the materials prepared cannot be classified as nanomaterials but composites of clay and agrogenic biomasses. The average particle size for the amino-functionalized adsorbents; *NPS-HYCA* and *N*PP-HYCA were observed to be more uniform than those of the parent adsorbents, *i*PS-HYCA and *i*PP-HYCA, respectively. Fig. 2E SEM images of *Carica papaya* seeds while Fig. 2F shows particles that are platy in nature consistent with Kaolinite clay.

Table 1
Energy Dispersive X-ray (EDX) Analysis for raw kaolinite, *i*PS-HYCA, *N*PS-HYCA, *i*PP-HYCA and *N*PP-HYCA adsorbents (*atomic percent composition of each atom in the adsorbents*).

Element	*i*PS-HYCA	*N*PS-HYCA	*i*PP-HYCA	*N*PP-HYCA
O	27.59	37.30	20.70	13.48
Al	25.86	4.68	6.78	12.22
Si	17.84	36.01	61.76	59.22
P	1.16	1.24	–	–
S	9.86	1.45	0.52	–
Cl	4.13	4.70	1.86	0.92
Ti	0.27	1.30	–	2.40
Fe	1.58	0.66	1.26	1.92
Zn	11.47	11.65	6.23	2.00
K	0.23	0.12	0.18	7.83

Note: These amounts are given in atomic percent composition of each atom in the adsorbents.

3.2.2. Elemental mapping and micro-analysis

The electron density analysis of the parent adsorbents (*i*PS-HYCA and *i*PP-HYCA) prepared under inert condition using the elemental mapping function of the SEM equipment (Supplementary data Figs. S3.1 and S3.2) shows that Zn was present in both adsorbents but was more evenly distributed in the *i*PS-HYCA adsorbent (Fig. S3.1, Table 1). The presence of Zn in these adsorbents indicates the successful doping of this metal into the composite adsorbents. The presence of Cl in both adsorbents (*i*PS-HYCA and *i*PP-HYCA) is as a result of the chloride salt of Zn used in the preparation of the adsorbent materials.

Iron and sulphur are chemical components of *Carica papaya* seeds and plantain peel (Okareh et al., 2015) which supports their presence in the elemental mapping images (Supplementary data Figs. S3.1 & S3.2) of both modified composite adsorbents. Conversely, *P* found in *Carica papaya* seed modified adsorbent is not

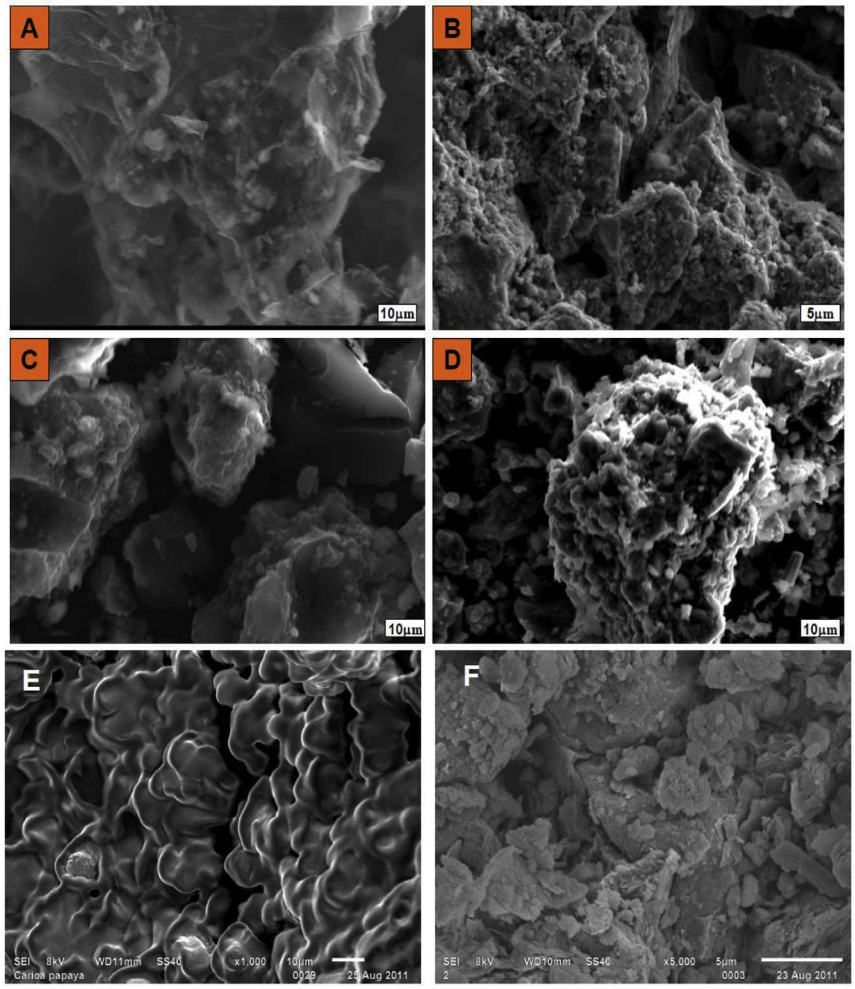

Fig. 2. Scanning Electron Microscopy images of (A) *i*PS-HYCA (B) *N*PS-HYCA (C) *i*PP-HYCA and (D) *N*PP-HYCA composite adsorbents (E) *Carica papaya* seed (F) Kaolinite Clay *Magnification*-(A) x1,500 (B) x5,000 (C) x1,500 (D) x1,000.

a chemical component of plantain peel. This makes *P* a unique element in *Carica papaya* seeds (Okareh et al., 2015).

However, with the functionalization of *i*PS-HYCA and *i*PP-HYCA adsorbents using an organosilane (AEPTS) to produce *N*PS-HYCA and *N*PP-HYCA adsorbents, the silica content of the functionalized materials increased (Table 1) as expected. Nitrogen is expectedly absent from the electron mapping images in supplementary data Figs S3.3 and 3.4. This is because the best accelerating voltage which provides the best efficiency for ionisation of nitrogen is 1 kV. However, the accelerating voltage used in this study for electron mapping analysis was (20 kV) and will thus produce less ionised nitrogen that could be detected by the SEM equipment (Stephant, 2016). Furthermore, elements of *Ti* present in our composite adsorbents from the clay can interfere with spectra lines of nitrogen (Love and V.D., 2001). This thus explains why nitrogen was seen in the FT-IR spectra as previously shown in Fig. 1 but not in the elemental mapping images as shown in supplementary data Figs S3.3 and 3.4.

3.3. X-ray diffraction analysis

The X-ray Diffraction (XRD) pattern of raw kaolinite, *i*PS-HYCA, *i*PP-HYCA, *N*PS-HYCA, and *N*PP-HYCA adsorbents are shown in Fig. 3. Peaks common to all the adsorbents include the quartz peaks at 21.09 and 50.08°, the Kaolinite peaks at 26.98, 45.90, and 55.00° and the peaks at 36.56, 39.26 and 42.47° (Fig. 3) indicating the presence of hexagonal wurtzite structure of Zn (Satyanarayana et al., 2012). A new peak showing hexagonal Wurtzite of ZnO was also observed at 27.44° (Satyanarayana et al., 2012) on the spectra of all composite adsorbents. This confirms the successful incorporation of Zn into the adsorbents. The highest intensities of the ZnO peak at 27.4° were observed with adsorbents prepared from plantain peels, *N*PP-HYCA and *i*PP-HYCA (Fig. 3), which indicates variations in the properties of the agrogenic materials used in the preparation of these adsorbents. However, there is a loss of the kaolinite peaks at 12.48° (001 reflection) and the peak at 25.01° (002 reflection) on the spectra of all agrogenic-modified adsorbents, suggesting a change in the crystalline structure of the kaolinite clay during the modification process. This supports our previous observation of the loss of out-phase hydroxyls of kaolinite (3698 cm^{-1}, 3669 cm^{-1}) and in-phase hydroxyl of kaolinite (3621 cm^{-1}) using the FTIR technique.

3.4. Point of zero charge (pH_{pzc})

The ease of adsorption of ions to the surface of adsorbents is dependent on the pH_{pzc} of such material. The pH_{pzc} can be used to understand and manipulate the net surface charge of adsorbent. If

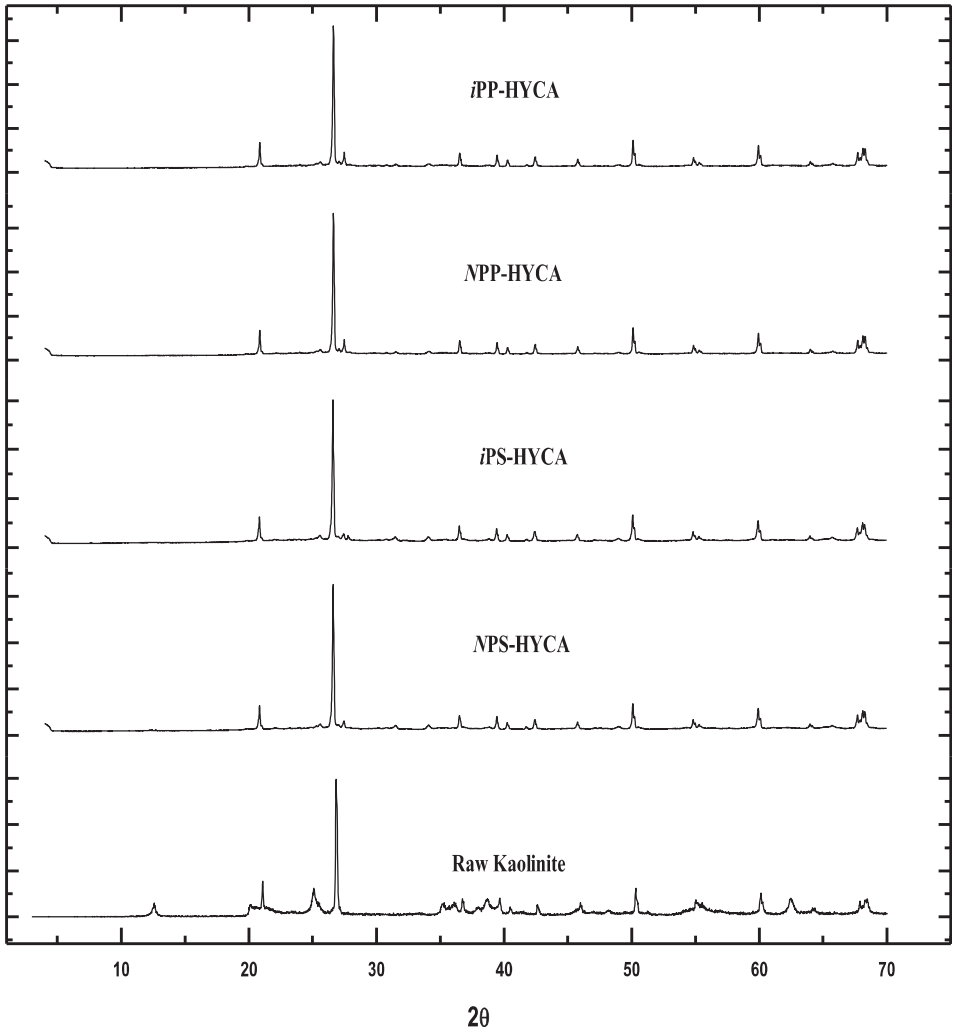

Fig. 3. X-ray Diffraction pattern for raw kaolinite, *N*PS-HYCA, *i*PS-HYCA, *N*PP-HYCA and *i*PP-HYCA composite adsorbents.

the pH of the solution containing the adsorbent is less than the pH_{pzc} of the composite adsorbent, the net surface charge of the adsorbent becomes positive because of the adsorption of excess H^+ and the net surface charge becomes negative when the pH of solution is higher than the pH_{pzc}, because of the desorption of H^+ (Li et al., 2008). The situation where the pH of solution is lower than the pH_{pzc} favours the adsorption of phosphate ions on the surface of the adsorbent which is predominantly positively charged due to coulombic attraction (Li et al., 2008).

The pH_{pzc} of the four adsorbents - *i*PS-HYCA, *N*PS-HYCA, *i*PP-HYCA and *N*PP-HYCA as shown in Fig. 4, are; 7.83, 6.91, 7.66 and 6.55 respectively. However, the pH_{pzc} for raw kaolinite used in this study is 4.98 (Unuabonah et al., 2013). This implies that all the modified adsorbents have a good pH range for the adsorption of phosphate ions with *i*PS-HYCA adsorbent having the best pH range since adsorption of anions in this study was carried out at pH range of 6.0–6.5 or less.

3.5. Adsorption studies

3.5.1. Kinetic analysis

The various parameters in kinetic models used in studying the kinetic data obtained from our study are shown in Table 2. For all the adsorbents prepared, the Brouers-Sotolongo Fractal, 'BSF(n,α)', kinetic model (Gaspard et al., 2006; Unuabonah et al., 2016; Brouers, 2014; Al-Musawi et al., 2017) used to describe very complex adsorption systems provided better fitness to experimental data than other kinetic models based on the Normalized Deviation (ND) and Normalized Standard Deviation (NSD) values obtained from the nonlinear regression modeling (Fig. 5a-d) of experimental data with the various kinetic models (Table 2). The *n* parameter in the BSF(n,α) kinetic model predicts a first order rate of uptake of phosphate ions on all prepared composite adsorbents except *i*PP-HYCA composite adsorbent. The BSF(n,α) kinetic model suggests that adsorption onto these adsorbents is via a complex mechanism including electrostatic, and weak Van der Waal forces (Guo et al., 2009; Al-Musawi et al., 2017).

Judging from the BSF(n,α) kinetic model data in Table 2, the $t_{1/2}$ (min) for the adsorption of phosphate onto the various composite adsorbents is in the increasing order of *N*PS-HYCA < *i*PS-HYCA < *N*PP-HYCA < *i*PP-HYCA indicating that the amino-functionalized composite adsorbents had better rate of phosphate uptake compared with the parent adsorbents. The *N*PP-HYCA adsorbent showed the best overall rate of uptake (Table 2). These results were also confirmed from PFOM and PSOM kinetic models where the overall rate of phosphate uptake improved by more than 8-fold for the composite adsorbents and as much as 40-fold in the case of *N*PS composite adsorbent, one of the amino-functionalized adsorbents (Table 2). Using the Normalized Deviation and Normalized Standard deviation models for determining the best model for rate uptake of phosphate adsorption onto these composite adsorbents, it is observed that the BSF(n,α) kinetic model best describe the kinetic data. This imply that the adsorption of phosphate onto these composite adsorbents involves a complex adsorption phenomenon which may include simultaneous chemical interaction between the solute and the chemical groups on the surface of the composites via electrostatic interactions, Van der Waals, hydrogen bounding, and ligand exchange (Guo et al., 2009). This might also suggest that the surface sites on these composite adsorbents are heterogeneous in nature.

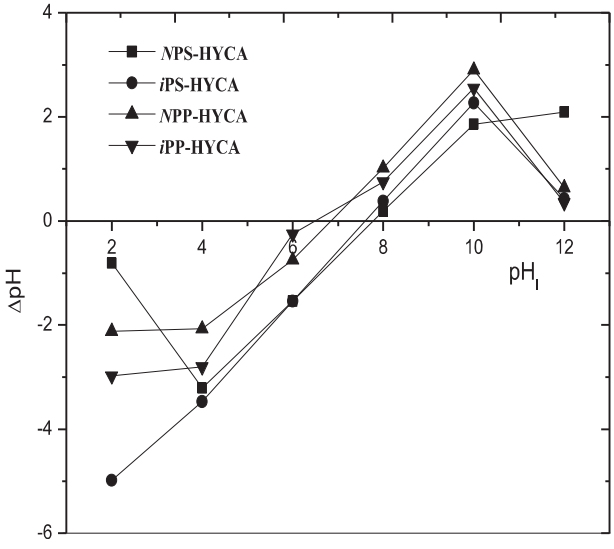

Fig. 4. pH_{pzc} of the amino functionalized adsorbents; *N*PS-HYCA and *N*PP-HYCA and the parent adsorbents; *i*PS-HYCA and *i*PP-HYCA.

3.5.2. Isotherm analysis

Experimental isotherm data obtained in this study were analysed with into four theoretical models-Freundlich (two-parameter isotherm model), Langmuir-Freundlich, Brouers-Sotolongo, and Sip isotherm models (three-parameter isotherm models). Plots of the fittings of these theoretical models compared to experimental data are shown in Fig. 6(a–d). The values of the parameters for the various theoretical models are presented in Table 3 a and b.

Then heterogeneity factor (*n*) in the Freundlich model can be used to indicate the degree of favorability of adsorption (Chung et al., 2015; Nemes and Bulgariu, 2016). The Freundlich constant, *n* should have values lying in the range of 1–10 for classification as favorable adsorption (Rao and Bhole, 2001). The values of *n* for all the adsorbents used in this study are all greater than 1 (Table 3) but less than 10 suggesting that the adsorption of phosphate ions onto these composites is favourable.

From the analysis of all the isotherms used in this study (Table 3), it can be deduced, with respect to *ND and NSD*, that the equilibrium data for the adsorption of phosphate ions onto these composite adsorbents is best described by the Freundlich isotherm model which predicts non-ideal and reversible adsorption on heterogeneous adsorption sites with no formation of monolayer on the adsorbent's surface (Olu-Owolabi et al., 2010). Since the Freundlich models do not predict adsorption maximum for an adsorbent (K_f is a constant indicative of the relative adsorption capacity of the adsorbent [Hamdaoui and Naffrecheoux, 2007]), the better model between Bruoers-Sotolongo and Langmuir-Freundlich models, which is Brouers-Sotolongo (BS) model, is then used to predict and discuss the adsorption capacities of the composites prepared in this study.

Considering Table 3 and using the BS model, it can be seen that amino-functionalization of *i*PS-HYCA and *i*PP-HYCA adsorbents increased their adsorption capacity from 59.16 to 67.37 mg/g and from 61.53 to 63.28 mg/g. The adsorption capacities of both agrogenic modified composite adsorbents (*i*PS-HYCA and *i*PP-HYCA) and amino-functionalized composite adsorbents (*N*PS-HYCA and *N*PP-HYCA) for phosphate adsorption are higher than those obtained for reduced steel slag and iron ore concentrate-2.74 mg/g at 30 °C (Wang et al., 2015), Ce (III)-impregnated crosslinked chitosan complex-45.37 mg/g at 30 °C (Hu et al., 2016), Mg-Al hydrotalcite-loaded kaolin clay-11.922 mg/g at 25 °C (Deng and Shi, 2015), Chitosan bead crosslinked with copper at 21 °C-53.6 mg/g (An et al., 2014), and Ce(III)-loaded gel from orange waste at 30 °C-13.94 mg/g (Biswas et al., 2007). When compared with commercial resins like the commercial cellulose-based resin (14.3 mg/g) Dowex 21K XLT

Table 2
Various kinetic data from model fittings for the adsorption of phosphate onto *i*PS-HYCA, *N*PS-HYCA, *i*PP-HYCA and *N*PP-HYCA composite adsorbents.

	PFOM			*PSOM*			*BSF(n,α)*		
	k_1	r^2	*ND (NSD)*	k_2	r^2	*ND/NSD*	*n*	r^2	*ND/NSD*
*N*PS-HYCA	1.20	0.9330	0.02 (0.06)	0.40	0.9615	0.005 (0.01)	1.05	0.9691	9.2 x E-5 (2.6 x E-4)
iPS-HYCA	0.07	0.9360	0.37 (1.05)	0.01	0.9436	0.14 (0.41)	1.00	0.9461	0.04 (0.10)
*N*PP-HYCA	2.8	0.9963	1.6 x E-4 (4.4 x E-4)	1.67	0.9983	4.9 x E-5 (1.4 x E-4)	1.04	0.9992	5.5 x E-7 (1.6 x E-6)
iPP-HYCA	0.29	0.8231	0.04 (0.12)	0.08	0.9260	0.01 (0.04)	2.29	0.9332	0.001 (0.03)

PSOM = pseudo-second-order model, PFOM = pseudo-first-order model, BSW = Brouers, Weron and Sotolongo model, k_1 (min^{-1}); k_2 ($g.mg^{-1}.min$); n is the fractional order of adsorption, $t_{1/2}$ = half-life of adsorption process (min), ND = Normalized Deviation, NSD = Normalized Standard Deviation.

(38.6 mg/g) and Amberlite IRA-400 (32.2 mg/g) (Hamoudi et al., 2007; Nur et al., 2016), it was also observed that the amino-functionalized adsorbents used in this study had better adsorption capacities.

Using the *b* values from the Langmuir-Freundlich model in this study (Table 3) to calculate the separation factor as shown in equation (4), it is observed that the adsorption of phosphate ions onto the composites prepared in this study is favourable since they are all below 1.0 (Unuabonah et al., 2007b) for all initial phosphate ions concentrations used in this study (Table 4).

3.6. Regeneration

There is economic and environmental importance in regenerating spent adsorbents for reuse rather than discarding them into the environment (Omorogie et al., 2016). Since interaction between phosphate ions and adsorbents in this study involves some electrostatic interaction, there is a need to use chemical reagents to enhance regeneration of the adsorbents, though care must be taken such that the chemical reagent does not end up blocking or destroying the sites after regeneration.

In this study, the various adsorbents were regenerated with 0.01 M and 0.1 M NaOH in 5 adsorption-desorption cycles. Fig. 7 shows the adsorption capacity after every regeneration cycle. From Fig. 7, the adsorbents all show decreasing adsorption capacity with increasing adsorption-desorption cycle. The amino-functionalized adsorbents (*N*PP-HYCA and *N*PS-HYCA) retained 84.1% and 94% respectively of their adsorption capacity after 5 adsorption-desorption cycles with 0.01 M NaOH and 37.5 and 35.5% for *i*PSHYCA and *i*PP-HYCA adsorbents. However, with 0.1 M NaOH, the plantain peel-based adsorbents (*i*PP-HYCA and *N*PP-HYCA) were favoured such that they retained ca. 33% of their adsorption capacity after 5 adsorption-desorption cycles as compared with between 5 and 35% for the *Carica papaya*-based adsorbents (*i*PS-

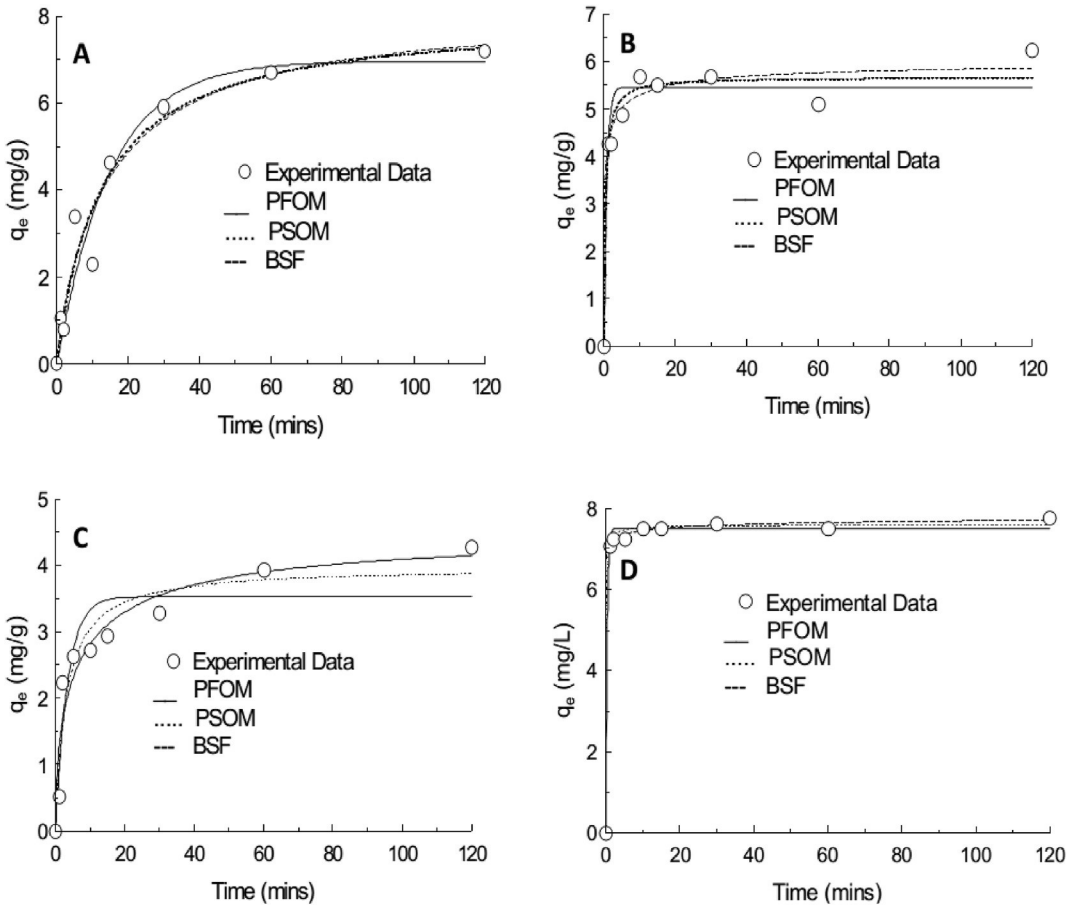

Fig. 5. Kinetic model plots for the adsorption of phosphate onto (A) *N*PS-HYCA,(B) *i*PS-HYCA, (C) *i*PP-HYCA and (D) *N*PP-HYCA composite adsorbents.

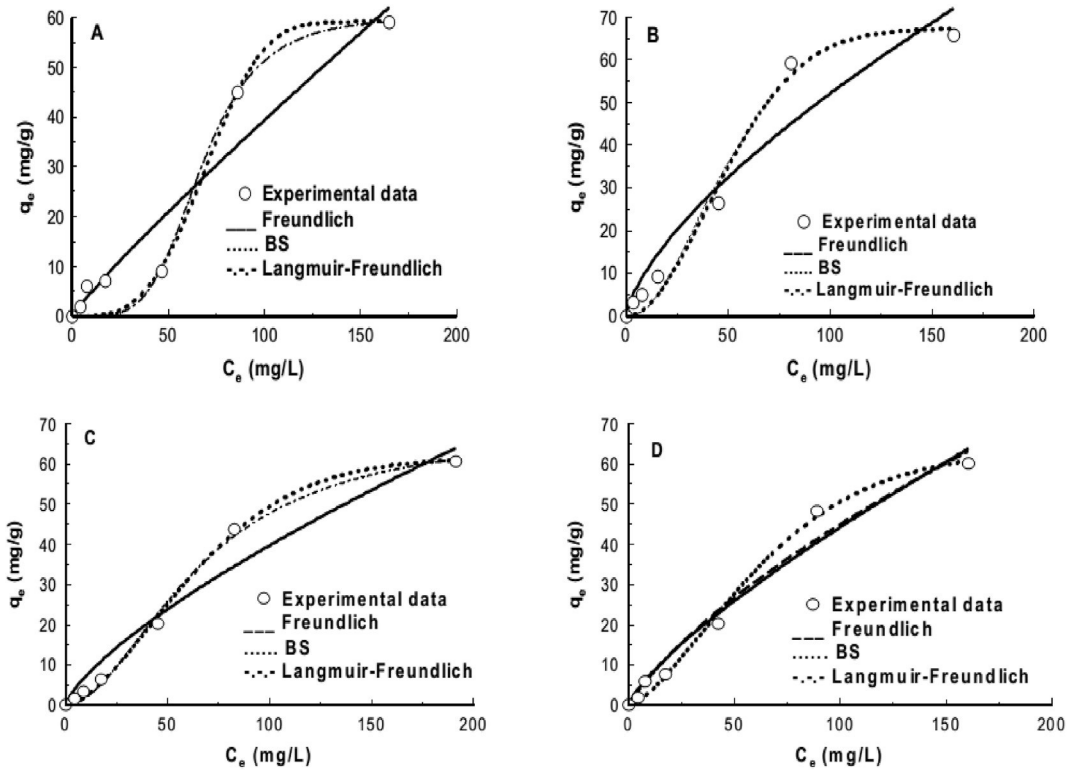

Fig. 6. Plots of isotherm model for the adsorption of phosphate onto (A) *i*PS-HYCA, (B) *N*PS-HYCA,(C) *i*PP-HYCA and (D) *N*PP-HYCA composite adsorbents.

Table 3
Freundlich, Langmuir-Fruendlich and Brouers Sotolongo isotherm model data for the adsorption of Phosphate onto *N*PS-HYCA, *i*PS-HYCA, *N*PP-HYCA and *i*PP-HYCA composite adsorbents.

	Freundlich				*Langmuir -Freundlich*					*BS*				
	K_f	n	r^2	*ND/NSD*	q_{max}	b	n	r^2	*ND/NSD*	q_{max}	k_{Bs}	α	r^2	*ND/NSD*
*N*PS-HYCA	2.27	1.47	0.9350	0.55/**1.33**	74.19	0.019	2.17	0.9760	0.96/**2.34**	67.37	4×10^{-4}	1.90	0.9848	0.91/**2.24**
iPS-HYCA	0.59	1.10	0.9293	0.10/**0.24**	60.34	0.015	4.42	0.9723	1.94/**4.75**	59.16	4.6×10^{-7}	3.36	0.9734	1.89/**4.62**
*N*PP-HYCA	1.27	1.30	0.9722	0.41/**0.99**	78.15	0.014	1.60	0.9908	0.46/**1.14**	63.28	0.0018	1.48	0.9935	0.45/**1.10**
iPP-HYCA	1.35	1.36	0.9613	0.67/**1.64**	69.48	0.015	1.89	0.9952	0.44/**1.07**	61.53	9×10^{-4}	1.63	0.9975	0.34/**0.84**

ND = Normalized Deviation, NSD = Normalized Standard Deviation.

HYCA and *N*PS-HYCA). This suggests that increasing the concentration of NaOH for regeneration purposes does negatively affect the efficiency of the composite adsorbents when they are regenerated and reused for phosphate removal in aqueous solution over several adsorption-desorption cycles. The 0.01 M NaOH is a better desorbing agent for phosphate-ladened adsorbents used in this study especially for the amino-functionalized adsorbents.

Furthermore, the adsorption-desorption studies suggest that the amino-functionalized adsorbents (*N*PS-HYCA and *N*PP-HYCA) are better candidates for phosphate capture and recovery from aqueous solution especially because of their better rate of uptake of phosphate from aqueous solution (Table 2) and phosphate adsorption capacity (Table 3). Increasing the concentration of NaOH could have lead to the damage of the structure of the composites or their active sites, thereby reducing their capacity after every adsorption-desorption cycle.

In studying the desorption kinetics for recovery of phosphate ions from these composite adsorbents, the First order two-site Desorption kinetic model (Willis et al., 1970; McLaren et al., 1986) and Modified Statistical Rate Theory (MSRT) Desorption Kinetic Model (Bashiri, 2011) were employed. The non-linear mathematical expressions for both models are shown in equations (3) and (4) respectively.

Table 5 and Fig. 8 shows the various parameters values from and desorption model plots for the First-Order Two-site Desorption and Modified Statistical Rate Theory (MSRT) Desorption Kinetic models. When the Normalized Standard Deviation (NSD) values are used to determine the kinetic desorption model that best describes the desorption kinetic data, it is observed that the First-Order Two-site Desorption kinetic model best describes the amino-functionalized adsorbents (*N*PP-HYCA and *N*PS-HYCA). This strongly indicates

Table 4
Separation factor values for the various composite adsorbents used in the adsorption of Phosphate Ions from aqueous solution.

C_o	K_R			
	*N*PS-HYCA	*i*PS-HYCA	*N*PP-HYCA	*iPP-HYCA*
5	0.913242	0.930233	0.934579	0.930233
10	0.840336	0.869565	0.877193	0.869565
20	0.724638	0.769231	0.78125	0.769231
50	0.512821	0.571429	0.588235	0.571429
100	0.344828	0.4	0.416667	0.4
Average	0.667173	0.708091	0.719585	0.708091

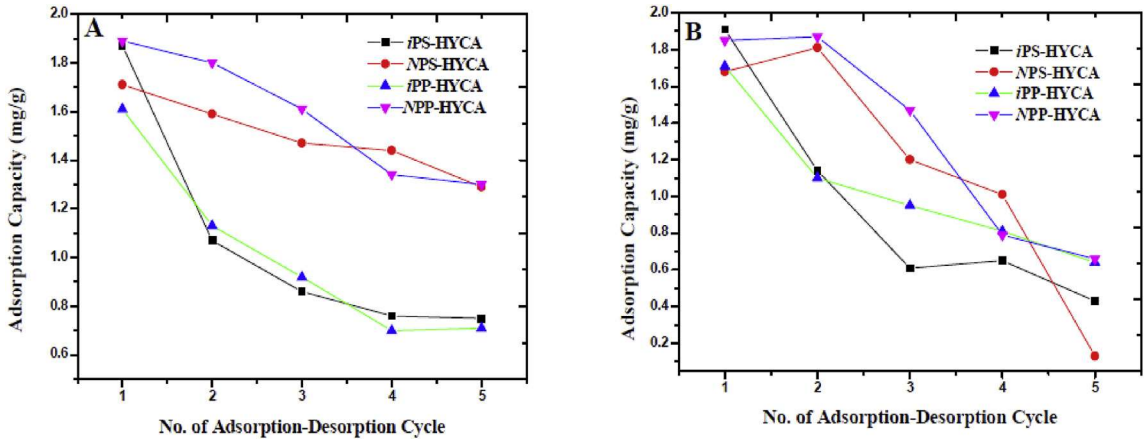

Fig. 7. Desorption of phosphate ions in 5 adsorption-desorption cycles for the various adsorbents where (A) 0.01 M NaOH and (B) 0.1 M NaOH.

Table 5
Fitting parameters of Desorption Kinetic Models of phosphate ion desorption from *i*PS-HYCA, *N*PS-HYCA, *i*PP-HYCA, and *N*PP-HYCA adsorbents using 0.01 M NaOH.

First Order 2-site Desorption Kinetic Model						
Adsorbent	C_1	$k_{1\ (min^{-1})}$	C_2	$k_{2\ (min^{-1})}$	r^2	NSD
*N*PS-HYCA	1.43	0.16	4.20	4×10^{-4}	0.9911	1.43 × E-5
*N*PP-HYCA	0.90	0.13	2.23	0.002	0.9774	0.0024
*i*PS-HYCA	1.49	0.11	3.71	4×10^{-4}	0.9867	1.56 × E-5
*i*PP-HYCA	2.22	2×10^{-4}	1.39	0.053	0.9959	0.00
Modified Statistical Rate Theory (MSRT) Desorption Kinetic Model						
Adsorbent	q_{des}	α	k_{des}	r^2	NSD	
*N*PS-HYCA	1.1	1.45	0.001	0.5442	0.0045	
*N*PP-HYCA	1.17	1.33	0.001	0.5817	0.053	
*i*PS-HYCA	1.05	0.92	0.003	0.8302	0.010	
*i*PP-HYCA	1.01	1.13	0.002	0.6843	0.037	

that amino functionalization of the composites does introduce another adsorption site onto the composite surfaces. This could be related to their better adsorption capacity on the unfunctionalized adsorbents. Additionally, it is observed that for First-Order Two-site Desorption kinetic model, the rate of phosphate desorption from 1st adsorption site is relatively faster than from the 2nd adsorption site as shown by the kinetic desorption rate constants, k_1 and k_2 in Table 4. Furthermore, the rate of phosphate ion desorption is more rapid with amino-functionalized composite adsorbents than with unfunctionalized composite adsorbents (Table 5).

We can understand the mechanism by which phosphate ions was adsorbed onto these composite adsorbents via the First-Order Two-site Desorption kinetic models. It is thus logical to suggest that adsorption onto amino-functionalized composite adsorbents will follow a mechanism wherein phosphate ions are adsorbed onto the two different sites simultaneously in support of the assumption made by the First-Order Two-site Desorption kinetic model (McLaren et al., 1986). It has been suggested that strong adsorption is a result of small rate constant [which in this case is site 2], while weak adsorption is a result of larger rate constant [which in this study is site 1] (Machida et al., 2004). Thus, there are more phosphate ions desorbed from site 2 (as depicted by C_2 in Table 5) than from site 1 (as represented by C_1 in Table 5).

It is noted that *N*PS-HYCA composite adsorbent showed a better rate of desorption of phosphate ions from aqueous solution than other three composite adsorbents prepare in this study. In ca. 25 min, desorption of phosphate ions from all composite adsorbents is 90% at equilibrium. The combination of C_1 and C_2 (Table 5) suggests that *N*PS-HYCA has a better adsorption efficiency for the removal of phosphate ions from aqueous solution than other three composite adsorbents. This result is mainly supported by our initial result

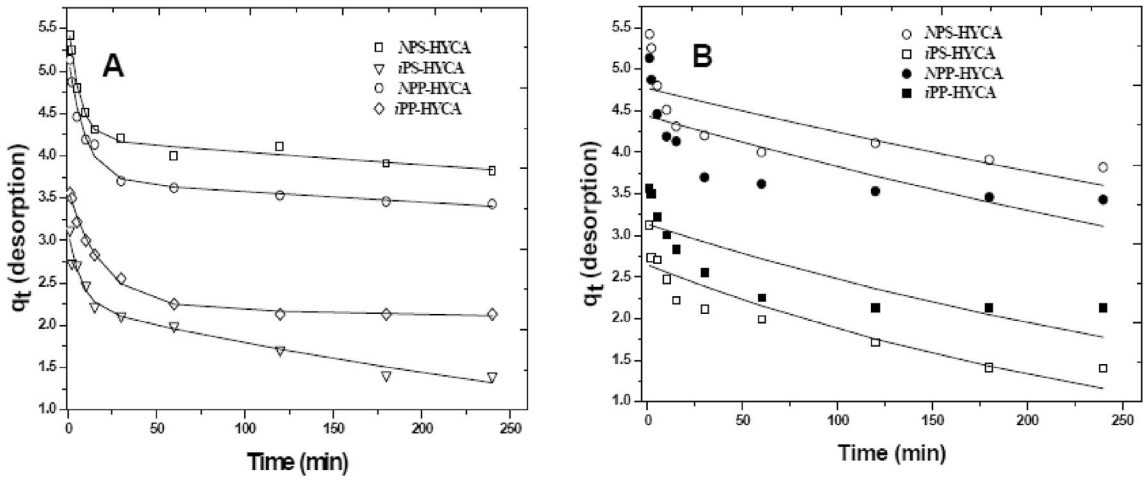

Fig. 8. Plots of kinetic models for phosphate ion desorption from the various composite adsorbents (A) First Order Two-site Desorption Kinetic Model (B) Modified Statistical Rate Theory Desorption Kinetic Model using 0.01 M NaOH.

from adsorption studies in this article which predicted *N*PS-HYCA composite adsorbent as the better adsorbent for phosphate adsorption than *N*PP-HYCA, *i*PP-HYCA and *i*PS-HYCA composite adsorbents. Furthermore, these regeneration results supports our earlier deduction that these composites adsorbents have heterogeneous adsorption sites as described by the Freundlich model that best described equilibrium data from this study.

These regeneration studies provides results that suggests that there could be an overall reduction in the cost of utilizing these composites especially *N*PS-HYCA composite adsorbent, in a large-scale water treatment system. Furthermore, these regeneration studies offer an advantage of recovery of phosphate that could be used in the agricultural sector. At the moment phosphate, a non-renewable resource shows a serious decline in its global reserves which obviously threatens the priority agenda for global food security (Cordell et al., 2009; Kunaschk et al., 2015).

4. Conclusion

The present work reports the successful preparation of Zn-doped hybrid clay adsorbents from two biomasses (*papaya* seed and plantain peel) and kaolinite clay. From the physicochemical characteristics of the composite adsorbents it can be concluded that the Zn exists as ZnO in the adsorbents.

The Brouers-Sotolongo Fractal (BSF) kinetic model provides a better fit to experimental data from kinetic studies for all adsorbents than other kinetic models based on the Normalised Deviation and Normalised Standard Deviation values obtained from the nonlinear regression modelling of experimental data. The BSF kinetic model suggests that adsorption onto these adsorbents is via a complex mechanism including electrostatic, and weak Van der Waal forces (Guo et al., 2009). The adsorption isotherm models showed that the adsorbents prepared were relatively effective in the adsorption of phosphate ions. The Brouers-Sotolongo isotherm model suggests that amino-functionalized *Carica papaya* hybrid clay composite adsorbent has the greater affinity for the phosphate ions. Regeneration of the amino-functionalized adsorbents was more effective with 0.01 M NaOH than 0.1 M NaOH and their capacity for phosphate removal after five consecutive adsorption-desorption cycles were 94.6%, and 84.13% for amino-functionalized *Carica papaya* hybrid clay and amino-functionalized *Musa paradisiaca* hybrid clay composite adsorbents respectively. The amino-functionalized adsorbents retained more of their adsorption capacity than their parent materials (37.5 and 35.5% for *Carica papaya* hybrid clay and *Musa paradisiaca* hybrid clay composite adsorbents respectively).

Desorption studies further confirmed the heterogeneous nature of the surfaces of the composite adsorbents used in this study via the First Order two-site Desorption Kinetic Model. The *N*PS-HYCA (hybrid clay prepared from *Carica papaya* seed and kaolinite and subsequently functionalized with an amino compound) has the best adsorption capacity for and rate of uptake of phosphate ions from aqueous solution.

Acknowledgement

This work was supported by The World Academy of Science (TWAS) with a grant (10-215 RG/CHE/AF/AC_G-UNESCO FR: 324028613). The authors acknowledge the support of the Redeemer's University, Nigeria, Department of Earth and Environmental Science, University of Potsdam, Potsdam, Germany and the Institute of Chemistry, Universität Potsdam, Germany for assistance in some analysis of samples.

Appendix A. Supplementary data

Supplementary data related to this article can be found at http://dx.doi.org/10.1016/j.jclepro.2017.06.160.

References

Adebowale, K.O., Unuabonah, E.I., Olu-Owolabi, B.I., 2005. Adsorption of some heavy metal ions on sulfate- and phosphate modified kaolin. Appl. Clay Sci. 29, 145–148.

Adebowale, K.O., Unuabonah, E.I., Olu-Owolabi, B.I., 2008. Kinetic and thermodynamic aspects of the adsorption of Pb^{2+} and Cd^{2+} ions on tripolyphosphate-modified kaolinite clay. Chem. Eng. J. 136, 99–107.

Al-Musawi, T.J., Brouers, F., Zarrabi, M., 2017. Kinetic modeling of antibiotic adsorption onto different nanomaterials using the Brouers–Sotolongo fractal equation. Environ. Sci. Pollut. Res. 24 (2017), 4048–4057.

An, B., Jung, K.Y., Lee, S.H., Lee, S., Choi, J.W., 2014. Effective phosphate removal from synthesized wastewater using copper-chitosan bead: batch and fixed-bed column studies. Water, Air Soil Pollut. 225 http://dx.doi.org/10.1007/s11270-11014-12050-11276.

Attia, S., Chaari, N., Chaabouni, S., 2015. Synthesis, crystal structure, and dielectric properties of (3-aminopropyl-imidazolium) pentachlorobismuthate (III) $[C_6H_{13}N_3]BiCl_5$. J. Clust. Sci. 26, 1343–1359.

Bacsik, Z., Ziadi, A.N., Zhao, G., Garcia-Bennett, A.E., Martín-Matute, B., Hedin, N., 2011. Mechanisms and kinetics for sorption of CO_2 on bicontinuous mesoporous silica modified with n-propylamine. Langmuir 27, 11118–11128.

Bashiri, H., 2011. Desorption kinetics at the solid/solution interface: a theoretical description by statistical rate theory for close-to-equilibrium systems. J. Phys. Chem. C 115, 5732–5739.

Bekele, W., Faye, G., Fernadez, N., 2014. Removal of nitrate ion from aqueous solution by modified Ethiopian bentonite clay. Int. J. Res. Pharm. Chem. 4, 192–201.

Bello, O.B., A, A.M., Mahmud, J., Afolabi, M.S., Ige, S.A., Abdulmaliq, S.Y., 2012. Evaluation of grain yield and agronomic characteristics in drought-tolerant maize varieties belonging to two maturing groups. J. Agric. Sci. 2, 70–74.

Biswas, K., Inoue, K., Ghimire, K.N., Ohta, S., Harada, H., Ohto, K., Kawakita, H., 2007. The adsorption of phosphate from an aquatic environment using metal-loaded orange waste. J. Colloids Interface Sci. 312, 214–223.

Brouers, 2014. The fractal (BSf) kinetics equation and its approximations. J. Mod. Phys. 5 (16), 1594–1598.

Calvo, A., Joselevich, M., Soler-Illia, G.J.A.A., Williams, F.J., 2009. Chemical reactivity of amino-functionalized mesoporous silica thin films obtained by co-condensation and post-grafting routes. Microporous Mesoporous Mater. 121, 67–72.

Chen, F., Wu, Q., Lü, Q., Xu, Y., Yu, Y., 2015. Synthesis and characterization of bifunctional mesoporous silica adsorbent for simultaneous removal of lead and nitrate ions. Sep. Purif. Technol. 151, 225–231.

Cheng, H., Liu, Q., Yang, J., Ma, S., Frost, R.L., 2012. The thermal behavior of kaolinite intercalation complexes: a review. Thermochim. Acta 545, 1–13.

Chung, H.-K., Kim, W.-H., Park, J., Cho, J., Jeong, T.-Y., 2015. Application of Langmuir and Freundlich isotherms to predict adsorbate removal efficiency or required amount of adsorbent. Journnal Industrial Eng. Chem. 28, 241–246.

Cordell, D., Drangert, J.-O., White, S., 2009. The story of phophorus: global food security and food thought. Glob. Environ. Change 19, 292–305.

Deng, L., Shi, Z., 2015. Synthesis and characterization of a novel Mg–Al hydrotalcite-loaded kaolin clay and its adsorption properties for phosphate in aqueous s. J. Alloy Compd. 637, 188–196.

Ebrahimi-Gatkash, M., Younesi, H., Shahbazi, H.,A., 2015. Amino-functionalized mesoporous MCM-41 silica as an efficient adsorbent for water treatment: batch and fixed-bed column adsorption of the nitrate anion. Appl. Water Sci. 1–15.

Elwakeel, K.Z., El-Bindary, A.A., El-Sonbati, A.Z., Hawas, A.R., 2016. Adsorption of toxic acidic dye from aqueous solution onto diethylenetriamine functionalized magnetic glycidyl methacrylate-N,N′-methylenebisacrylamide. RSC Adv. 6, 3350–3361.

Farmer, V.C., Russell, J.D., 1964. The Infrared spectra of layered silicates. Spectrochem. Acta 20, 1149–1173.

Frost, R.L., Vassallo, A.M., 1996. The dehydroxylation of the kaolinite clay minerals using Infrared emission spectroscopy. Clays Clay Mineral. 44, 635–651.

Ganesapillai, M., Simha, P., 2015. The rationale for alternative fertilization: equilibrium isotherm, kinetics and mass transfer analysis for urea-nitrogen adsorption from cow urine. Resour. Effic. Technol. 1, 90–97.

Gaspard, S., Altenor, S., Passe-Coutrin, N., Ouensanga, A., Brouers, F., 2006. Parameters from a new kinetic equation to evaluate activated carbons efficiency for water treatment. Water Res. 40, 3467–3477.

Ghorbani, M., Nowee, S.M., Ramezanian, N., F, R., 2016. A new nanostructured material amino functionalized mesoporous silica synthesized via co-condensation method for Pb(II) and Ni(II) ion sorption from aqueous solution. Hydrometallurgy 161, 117–126.

Greenberg, A.E., Clesceri, L.S., Eaton, A.D., 1992. Standard Methods for the Examination of Wastewater, Inorganic Nonmetals (4000). American Public Health Association (APHA).

Guo, L., Liu, J., Xing, G., Wen, Q., 2009. Adsorption and desorption of zinc(II) on water-insoluble starch phosphates. J. Appl. Polym. Sci. 111, 1110–1114.

Hamdaoui, O., Naffrecheoux, E., 2007. Modeling of adsorption isotherms of phenol and chlorophenols onto granular activated carbon Part I. Two-parameter models and equations allowing determination of thermodynamic parameters. J. Hazard. Mater. 147, 381–394.
Hamoudi, S., El-Nemr, A., Belkacemi, K., 2010. Adsorptive removal of dihydrogenphosphate ion from aqueous solutions using mono, di- and tri-ammonium-functionalized SBA-15. J. Colloid Interface Sci. 343, 615–621.
Hamoudi, S., Saad, R., Belkacemi, K., 2007. Adsorptive removal of phosphate and nitrate anions from aqueous solutions using ammonium-functionalized mesoporous silica. Ind. Eng. Chem. Res. 8806–8812.
Hu, P., Liu, Q., Wang, J., Huang, R., 2016. Phosphate removal by Ce(III)-Impregnated crosslinked chitosan complex from aqueous solutions. Polym. Eng. Sci. http://dx.doi.org/10.1002/pen.24383.
Huang, W., Wang, S., Zhu, Z., Li, L., X, Y., Rudolph, V., Haghseresht, F., 2008. Phosphate removal from wastewater using red mud. J. Hazard. Mater. 158, 35–42.
Kunaschk, M., Schmalz, V., Dietrich, N., Dittmar, T., Worch, E., 2015. Novel Regeneration methhod for phosphate loaded granular ferric(hydr)oxide-A contribution to phosphorus recycling. Water Res. 71, 219–226.
Lee, J.Y., Chen, C.H., Cheng, S., Li, H.Y., 2016. Adsorption of Pb(II) and Cu(II) metal ions on functionalized large-pore mesoporous silica. Int. J. Environ. Sci. Technol. 13, 65–76.
Li, J., Miao, X., Hao, Y., Zhao, J., Sun, X., Wang, L., 2008. Synthesis, amino-functionalization of mesoporous silica and its adsorption of Cr(VI). J. Colloid Interface Sci. 318, 309–314.
Lin, S.H., Juang, R.S., 2002. Removal of free and chelated Cu(II) ions from water by a nondispersive solvent extraction process. Water Res. 36, 3611–3619.
Love, G., V.D, S., 2001. Electron probe microanalysis using soft X-rays - a review. Part 1: instrumentation, spectrum processing and detection sensitivity. J. Microsc. 201, 1–32.
Machida, M., Kikuchi, Y., Aikawa, M., Tatsumoto, H., 2004. Kinetics of adsorption and desorption of Pb(II) in aqueous solution on activated carbon by two-site adsorption model. Colloids Surfaces A Physicochem. Eng. Aspects 240, 179–186.
McLaren, R.G., Lawson, D.M., Swift, R.S., 1986. Sorption and desorption of cobalt by soils and soil components. J. Soil Sci. 37, 413–426.
Moore, D.M., Reynolds, R.C., 1989. X-ray Diffraction and the Identification and Analysis of Clay Minerals. Oxford University Press, Cambridge, U.K. Jr.
Morales, V., Idso, M.N., Balabasquer, M., Chmelka, B., García-Muñoz, R.A., 2016. Correlating surface-functionalization of mesoporous silica with adsorption and release of pharmaceutical guest species. J. Phys. Chem. C 120, 16887–16898.
Najafi, M., Yousefi, Y., Rafati, A.A., 2012. Synthesis, characterization and adsorption studies of several heavy metal ions on amino-functionalized silica nano hollow sphere and silica gel. Sep. Purif. Technol. 85, 193–205.
Nakanishi, K., Tomita, M., Kato, K., 2014. Synthesis of amino-functionalized mesoporous silica sheets and their application for metal ion capture. J. Asian Ceram. Soc. 3, 70–76.
Nemes, L., Bulgariu, L., 2016. Optimization of process parameters for heavy metals biosorption onto mustard waste biomass. Open Chem. 14, 175–187.
Nur, T., Loganathan, P., Kandasamy, J., Vigneswaran, S., 2016. Phosphate adsorption from membrane bioreactor effluent using Dowex 21K XLT and recovery as struvite and hydroxyapatite. Int. J. Environ. Res. Public Health 13, 1–12.
Ogundiran, M.B., Winjobi, F.A., 2015. The potential of binary blended geopolymer binder containing Ijero-Ekiti calcined kaolin clay and ground waste window glass. Afr. J. Pure Appl. Chem. 9, 159–166.
Okareh, O.T., Adeolu, A.T., Adepoju, O.T., 2015. Proximate and mineral composition of plantain (*Musa Paradisiaca*) wastes flour; a potential nutrients source in the formulation of animal feeds. Afr. J. Food Sci. Technol. 6, 53–57.
Oladoja, N.A., Adelagun, R.O.A., Ahmad, A.L., Ololade, I.A., 2015. Phosphorus recovery from aquaculture wastewater using thermally treated gastropod shell. Process Saf. Environ. Prot. 98, 296–308.
Oladoja, N.A., Adelagun, R.O.A., Ololade, I.A., Anthony, E.T., Alfred, M.O., 2014. Synthesis of nano-sized hydrocalumite from a Gastropod shell for aqua system phosphate removal. Sep. Purif. Technol. 124, 186–194.
Olu-Owolabi, B.I., Popoola, D.B., Unuabonah, E.I., 2010. Removal of Cu^{2+} and Cd^{2+} from aqueous solution by Bentonite clay modified with binary mixture of goethite and humic acid. Water, Air Soil Pollut. 211, 459–474.
Oliveira, M., Machado, A.V., Nogueira, R., 2012. Phosphorus removal from eutrophic waters with aluminium hybrid nanocomposite. Water, Air & Soil Pollut. 223, 4831–4840.
Olu-Owolabi, B.I., Unuabonah, E.I., 2011. Adsorption of Zn^{2+} and Cu^{2+} onto sulphate and phosphate-modified bentonite. Appl. Clay Sci. 51, 170–173.
Omorogie, M.O., Babalola, J.O., Unuabonah, E.I., 2016. Regeneration Strategies for spent solid matrices used in adsorption of organic pollutants from surface water: a critical review. Desalination Water Treat. 57, 518–544.
Puglisi, A., Annunziata, R., Benaglia, M., Cozzi, F., Gervasini, A., Bertacche, V., Sala, M.C., 2009. Hybrid inorganic-organic materials carrying tertiary amine and thiourea residues tethered on mesoporous silica nanoparticles: synthesis, characterization, and Co-Operative catalysis. Adv. Synthesis Catal. 351, 219–229.
Raevskaya, A.E., Stroyuk, O.L., Solonenko, D.I., Dzhagan, V.M., Lehmann, D., Ya Kuchmiy, S., Plyusnin, V.F., Zahn, D.R.T., 2014. Synthesis and luminescent properties of ultrasmall colloidal CdS nanoparticles stabilized by Cd(II) complexes with ammonia and mercaptoacetate. J. Nanoparticle Res. 16, 2650–2655.
Rao, M., Bhole, A.G., 2001. Chromium removal by adsorption using fly ash and bagasse. J. Indian Water Works Assoc. XXXIII (1), 97–100.
Satyanarayana, T., Srinivasa, R.K., Gunnam, N., 2012. Synthesis, Characterization, and Spectroscopic Properties of ZnO Nanoparticles. ISRN Nanotechnology.
Shen, H., Wang, Y.-T., 1994. Biological reduction of chromium by *E. coli*. J. Environ. Eng. 120, 560–571.
Simha, P., Zabaniotou, A., Ganesapillai, M., 2017. Continuous urea–nitrogen recycling from human urine: a step towards creating a human excreta based bio–economy. J. Clean. Prod. http://dx.doi.org/10.1016/j.jclepro.2017.01.062.
Stephant, N., 2016. In: Why during SEM-EDX We Cannot Detect Nitrogen However on the Element Map Nitrogen Is Detected what Reason Could Someone Explain. Researchgate.
Tu, S., Lv, F., Hu, P., Meng, Z., Ran, Y., Zhang, Y., 2015. Preparation of amine-modified silica foams and their adsorption behaviors toward TNT red water. Colloids Surfaces A Physicochem. Eng. Aspects 481, 493–499.
Ugurlu, A., Salman, B., 1998. Phosphorus removal by fly ash. Environ. Int. 24, 911–918.
Unuabonah, E.I., Adebowale, K.O., Olu-Owolabi, B.I., 2007a. Kinetic and Thermodynamic studies of the adsorption of lead (II) ions onto phosphate-modified kaolinite clay. J. Hazard Material 144, 386–395.
Unuabonah, E.I., Olu-Owolabi, B.I., Adebowale, K.O., Ofomaja, A.E., 2007b. Adsorption of lead and cadmium ions from aqueous solutions bytripolyphosphate-impregnated Kaolinite Clay. Colloids Surf. A: Physicochem. Eng. Asp. 292, 202–211.
Unuabonah, E.I., Günter, C., Weber, J., Lubahn, S., Taubert, A., 2013. Hybrid clay: a new highly efficient adsorbent for water treatment. ACS Sustain. Chem. Eng. 1, 966–973.
Unuabonah, E.I., Olu-Owolabi, B.I., Adebowale, K.O., 2016. Competitive adsorption of metal ions onto goethite–humic acid-modified kaolinite clay. Int. J. Environ. Sci. Technol. 1–15.
Unuabonah, E.I., Olu-Owolabi, B.I., Oladoja, N.A., Ofomaja, A.E., Yang, L.Z., 2010. Pb/Ca ion exchange on Kaolinite clay modified with phosphates. J. Soils Sediments 10, 1103–1114.
Vilar, V., Botelho, C., Bonaventura, R., 2007. Modeling equilibrium and kinetics of metal uptake by algal biomass in continuous stirred and packed bed adsorbers. Adsorption-Journal Int. Adsorpt. Soc. 13, 587–601.
Wang, H., Shen, S., Liu, L., Ji, Y., Wang, F., 2015. Effective adsorption of phosphate from wastewaters by big composite pellets made of reduced steel slag and iron ore concentrate. Environ. Technol. 36, 2835–2846.
Willis, B.G., Woodruff, W.H., Frysinger, J.R., Margerum, D.W., Pardue, H.L., 1970. Simultaneous kinetic determination of mixtures by on-line regression analysis. Anal. Chem. 42, 1350–1355.
Xie, J., Lai, L., Lin, L., Wu, D., Zhang, Z., Kong, H., 2015. Phosphate removal from water by a novel zeolite/lanthanum hydroxide hybrid material prepared from coal fly ash. J. Environ. Sci. Health, Part A 50, 1298–1305.
Xin, X., Wei, Q., Yang, L., Feng, R., Chen, G., Du, B., Li, H., 2012. Highly efficient removal of heavy metal ions by amine-functionalized mesoporous Fe_3O_4 nanoparticles. Chem. Eng. J. 184, 132–140.
Zhang, L., Wan, L., Chang, N., Liu, J., Duan, C., Zhou, Q., Li, X., Wang, X., 2011. Removal of phosphate from water by activated carbon fiber loaded with lanthanum oxide. J. Hazard. Mat. 190, 848–855.
Zhang, Z., Liu, H., Wu, L., Lan, H., Qu, J., 2015. Preparation of amino-Fe(III) functionalized mesoporous silica for synergistic adsorption of tetracycline and copper. Chemosphere 138, 625–632.